Research Article | Vol. 28, No. 26 / 21 December 2020 / Optics Express 38698
Optics EXPRESS

Coherent transfer of topological interface states

P. COMARON,[1,*] V. SHAHNAZARYAN,[1,2] AND M. MATUSZEWSKI[1]

[1] Institute of Physics, Polish Academy of Sciences, Al. Lotnikow 32/46, 02-668 Warsaw, Poland
[2] ITMO University, St. Petersburg 197101, Russia
[*] paolocomaron@gmail.com

Abstract: We demonstrate the controlled coherent transfer of topological interface states in a one-dimensional non-Hermitian chain of interacting Bose-Einstein condensates. The topological protection stems from a spatially patterned pump in an open-dissipative system. As a test bed setup of the proposed phenomenon, we consider a chain of coupled micropillars with embedded quantum wells, possessing exciton-polariton resonances. The transfer of an interface state is driven by spatially localised, adiabatic pump modulation in the vicinity of the interface state. The stochastic calculations prove the coherent nature of the interface state transfer. For appropriate system parameters the coherence degree is preserved after multiple transitions, paving the way towards long-range transfer of a coherent quantum state.

1. Introduction

Topological insulators (TI) are a class of materials that possess an energy bandgap and topologically protected low energy states [1,2]. Topological protection in these systems stems from the symmetry of the bulk, which is quantified by means of topological invariants. Bulk-boundary correspondence results in the protection of edge states, which hold promise for applications in dissipation-less communications and quantum computing.

While in standard TIs non-trivial topology results from the properties of a Hermitian Hamiltonian, recently a class of non-Hermitian topological systems attracted great interest [3]. These are of particular relevance to photonics, where open-dissipative effects are prevalent. The latter, on one side, makes photonic systems an optimal platform for probing phenomena emerging specifically in the non-Hermitian domain. In this context phenomena such as lasing of topological states have been demonstrated [4,5]. On the other side, recently it was proposed to use the non-Hermiticity of photonics as an efficient tool for controlling the topological properties of the system. This can be reached, particularly, through asymmetric coupling coefficients [6] or spatial modulation of gain-loss ratio in each site [7–9]. Arguably, the greatest fundamental interest lies in the investigation of topological states that result solely from the non-Hermiticity of the system, since these have no counterparts in the Hermitian case [10–17].

In this paper, we consider the question whether non-Hermiticity can be used for precise control of topological states. Similarly to electrons in crystalline media, electromagnetic waves in periodically patterned photonic structures form energy bands, which can lead to appearance photonic edge states [4,5,18–27]. The presence of topological protection suppresses the backscattering on disorder, thus generating an energy-efficient propagation channel. However, in such a setting there is no convenient way to externally control the direction or velocity of the wave packet. On the other hand, photonic implementations of non-Hermitian Hamiltonians relying on spatial modulation of external pumping allow to efficiently tune certain terms of the Hamiltonian. This opens the way to the control of topological states, which can be crucial for future applications, such as scattering-free optical interconnects, quantum computation, or Majorana state braiding [28].

The distinctive peculiarities of photonic TIs can be further extended in the regime of strong-light matter coupling in a microcavity with embedded quantum wells [29]. The emerging

#409715 https://doi.org/10.1364/OE.409715
Journal © 2020 Received 9 Sep 2020; accepted 3 Nov 2020; published 8 Dec 2020

Optics EXPRESS

hybrid quasiparticles, called exciton-polaritons, are interacting via their excitonic component, allowing thus to achieve a strong nonlinear response in comparison to other photonic systems. Typically, etching of cavity is used to fabricate an array of coupled micropillars, mimicking the structure of a tight-binding Hamiltonian. In the majority of existing theoretical proposals [30–44] and experimental realizations [45–49] topological order emerges from Hermitian band engineering, whereas open-dissipative nature of the system serves only to create a non-equilibrium Bose-Einstein condensate of polaritons in each micropillar.

As we demonstrated recently, topological protection in a chain of coupled polariton micropillars can be achieved solely via the spatial modulation of external pump [9] in a system with equal hopping coefficients. Topological characterization of the system revealed the existence of multiple phases, with different number of end states. Here, we show that at the boundary of such phases a non-decaying topological interface state can be created. By means of adiabatic switching of the pump pattern, we induce a controllable transfer of the interface state. Moreover, by calculating the first-order correlation function, we demonstrate that such transfer is of coherent nature. We determine the optimal conditions for the coherent transfer, such as time dependence of the spatial pump pattern and the switching time. Our results are confirmed by stochastic simulations within the truncated Wigner approximation, which include the effect of quantum fluctuations.

2. Model

2.1. Hamiltonian

The structure we consider consists of a chain of unit cells, each including four sites. The on-site potential within each cell is spatially modulated. The bulk of the chain is analogous as in our previous work [9]. Here, we consider interface states which emerge at the boundary between two phases supporting a different number of edge states. The Hamiltonian of the system reads

$$\begin{aligned}\hat{H} = e^{i\theta}\sum_{n=1}^{n_b}\left(g_1\hat{a}_n^\dagger\hat{a}_n - g_2\hat{b}_n^\dagger\hat{b}_n - g_1\hat{c}_n^\dagger\hat{c}_n + g_2\hat{d}_n^\dagger\hat{d}_n\right)\\ +e^{i\theta}\sum_{n=n_b+1}^{N}\left(g_3\hat{a}_n^\dagger\hat{a}_n - g_4\hat{b}_n^\dagger\hat{b}_n - g_3\hat{c}_n^\dagger\hat{c}_n + g_4\hat{d}_n^\dagger\hat{d}_n\right)\\ +\kappa\sum_{n=1}^{N}\left(\hat{b}_n^\dagger\hat{a}_n + \hat{c}_n^\dagger\hat{b}_n + \hat{d}_n^\dagger\hat{c}_n + \hat{a}_{n+1}^\dagger\hat{d}_n + H.c.\right),\end{aligned} \tag{1}$$

where N is the total number of unit cells, and n_b denotes the boundary unit cell between the two phases. Here $g_i e^{i\theta}$ denotes the on-site potential, which is generally a complex valued quantity (g_i and θ are real numbers). κ denotes the nearest neighbour hopping rate between the sites, which is uniform throughout the chain. Such a Hamiltonian corresponds, in particular, to an exciton-polariton system of coupled micropillars, where the imaginary part of the on-site potential results from an external incoherent pump, and the real part stands for the Coulomb interaction between particles in a polariton condensate and in an incoherent reservoir [9]. The parameter θ describes the ratio of real and imaginary components of the on-site potential, and thus is determined by the material composition and design of the system, including the exciton-polariton detuning.

2.2. Interface states and protocol of the transition

It was previously shown [9] that in the homogeneous case (i.e. $g_3 = g_1, g_4 = g_2$) the Hamiltonian (1) can exhibit one or two pairs of edge states, odd number of edge states, or be topologically trivial. In order to perform dynamical study of interface state behaviour in a dissipative system, one needs a single topological state to be the only non-decaying eigenstate. Hence, the imaginary

Optics EXPRESS

part of interface state eigenenergy needs to be the highest among all the eigenmodes. Such a situation can be reached via judicious choice of parameters, with the interface state appearing on the boundary of two topological phases, exhibiting one and two pairs of edge states, respectively. Particularly, here we choose the values of parameters $g_1 = -2\kappa$, $g_3 = 2\kappa$, $g_2 = g_4 = \kappa$, $\theta = \pi/3$, the length of the chain $N = 40$, and the boundary unit cell $n_b = 10$. We also uniformly reduce by $-i\gamma$ the on-site potentials of the system, so that only the interface state has positive imaginary part of eigenvalue. The shape of the interface state and the imaginary part of the energy spectrum are shown in Fig. 1(a), left and right panels, respectively, where $\gamma = 1.35\kappa$. Notably, the interface state is "M"-shaped, almost completely localized in 5 sites, and centred exactly around the boundary site between the two phases.We proceed with the study of coherent transfer of an interface state. The protocol of transfer consists of several steps, which are illustrated as follows. For a better understanding, let us consider first the evolution in the mean field regime, as sketched in Fig. 1(b). We start with a random distribution, and eventually reach a nonequilibrium steady state configuration, if growth saturation is present. The latter naturally emerges in any system where pumping has a limited capacity. This state is labelled as "initial" in Fig. 1(b). Then, we gradually modify the pump pattern at the boundary of two phases, and thus shift the boundary by one unit cell. In the beginning of the "transient" stage the existing interface state ceases to be a non-decaying mode, and rapidly becomes depleted. The new interface state emerges at the new boundary between the phases, and becomes populated. Steady state of the configuration hosting the new shifted interface state is eventually reached in the "final" state. Yet, such a combination of two independent processes does not lead to a transfer of macroscopic population which retains the coherence of the condensate. To avoid this scenario, during the transition process we apply extra pump to the region of existing interface state, which replenishes the decaying population. In this case we find that the interface state is indeed shifted by one unit cell.

To verify this, we perform stochastic simulations, and calculate the spatially and temporally resolved degree of coherence between interface states at the initial and final stages of the process. The evolution of condensate can be described by a stochastic discrete Gross-Pitaevskii equation [9], in which sites are coupled to each other due to the presence of hopping. The corresponding set of equations reads

$$i\hbar \mathrm{d}\psi_{n,i} = \left[-\kappa \sum_{\langle nn \rangle} \psi_{n',i'} + \epsilon_{n,i}(t)\psi_{n,i} - \Gamma_{n,i}\left(1 + i\tan\theta\right)|\psi_{n,i}|^2\psi_{n,i} \right] \mathrm{d}t + \xi_{n,i}(t), \tag{2}$$

where $\langle nn \rangle$ runs over the nearest neighbours, $n \in [1, N]$ and $i = A, B, C, D$ is the sub-lattice label. Here $\psi_{n,i}(t)$ is the condensate amplitude in the corresponding site, $\epsilon_{n,i}(t) = g_i e^{i\theta} - i\gamma$ (see Appendix A for details of the derivation). The parameter $\Gamma_{n,i}$ describes the nonlinearity in each site. The last term denotes a Gaussian white noise with correlations $\langle \xi_{ni}(t)\xi^*_{n'i'}(t')\rangle = \delta_{nn'}\delta_{ii'}\delta_{tt'}\beta^2(g_i \sin\theta - \gamma + \gamma_c)/d$ accounting for quantum fluctuations. It should be noted that the chosen noise amplitude corresponds to the particular case of exciton-polariton condensates, but in principle an analogous definition can be given for other related systems [50,51]. Here the parameter β is the dimensionless scaling factor describing the scaling of noise amplitude, γ_c and d characterize polariton decay rate and the diameter of the pillar, respectively. The derivation of nonlinearity and noise rates for the polariton model are presented in Appendix A.

We subdivide the period of switching process T_{tr} into three parts of equal duration. At first, we gradually increase by $i\sigma$ the on-site potential of two last sites of the boundary unit cell n_b, which is the leftmost cell in Fig. 1(b). Second, we perform the switching of on-site potentials in the boundary unit cell $n_b + 1$. Finally, in the third step we gradually turn off the supporting potential. Hence, the majority of on-site potentials in Eq. (2) are time-independent, except the vicinity of interface state. Particularly, for the unit cell $n_b + 1$, the middle cell in Fig. 1(b), the

Optics EXPRESS

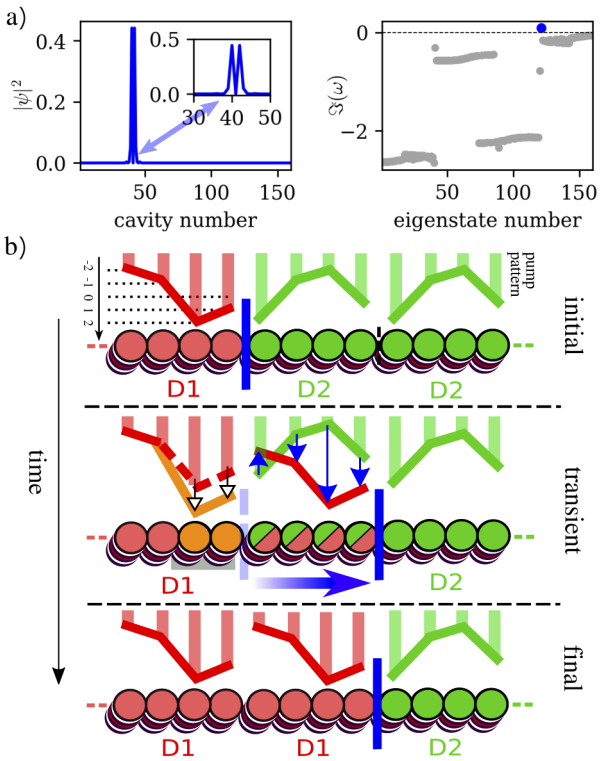

Fig. 1. (a) The spatial density distribution of an eigenstate corresponding to a topological interface state emerging on the boundary between two topological phases (left panel). The imaginary parts of eigenvalues of Hamiltonian (1) in units of κ (right panel). The blue dot corresponds to interface state. Here a uniform reduction of eigenvalues by $-i\gamma$ is applied. (b) The sketch of boundary between the topological phases and its temporal evolution. In transient regime the pump rates in middle unit cell are gradually modified, resulting in shifting the boundary to one unit cell. In the transient regime a supporting potential is applied to the boundary pillars (marked by orange), which protects the initial interface state from depletion during the transfer of the state.

switching is given by

$$\epsilon_{n_b+1,A[C]} = \left(\pm g_3 + \frac{\pm(g_1 - g_3)}{1 + e^{-(t-\tau_1)/\Delta\tau}}\right) e^{i\theta} - i\gamma, \tag{3}$$

$$\epsilon_{n_b+1,B[D]} = \left(\pm g_4 + \frac{\pm(g_2 - g_4)}{1 + e^{-(t-\tau_1)/\Delta\tau}}\right) e^{i\theta} - i\gamma, \tag{4}$$

where + [−] signs correspond to sites (A,B), [(C,D)], respectively. In addition, for the last two sites of unit cell n_b we have

$$\epsilon_{n_b,C} = -g_1 e^{i\theta} + \frac{\sigma(i + \cot\theta)}{1 + e^{(t-\tau_2)/\tau}} \left(1 - \frac{1}{1 + e^{(t-\tau_0)/\Delta\tau}}\right), \tag{5}$$

$$\epsilon_{n_b,D} = g_2 e^{i\theta} + \frac{\sigma(i + \cot\theta)}{1 + e^{(t-\tau_2)/\Delta\tau}} \left(1 - \frac{1}{1 + e^{(t-\tau_0)/\Delta\tau}}\right). \tag{6}$$

Here $\tau_2 - \tau_0 = T_{\rm tr}$, $\tau_1 = \tau_0 + T_{\rm tr}/3$, and $\Delta\tau$ characterizes the transition rate, which we choose as $\Delta\tau \approx T_{\rm tr}/45$. The dependence of imaginary part of the on-site potentials is shown in Fig. 2.

Optics EXPRESS

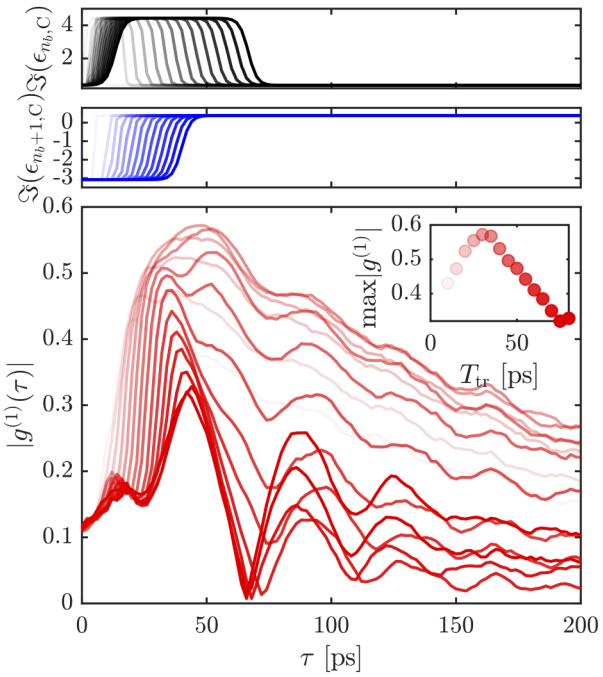

Fig. 2. The dependence of interface state coherence on switching speed in the case where interface state is shifted by one unit cell. Top panel: the temporal dependence of supporting pump applied to the existing interface state. Middle panel: temporal dependence of pump rates in the boundary unit cell. The pump values are in units of κ. Bottom panel: first order correlation function defined by Eq. (8) for different transition times $T_{\rm tr}$. The inset illustrates the maxima of coherence at different transition times. The colour tones in plots correspond to values of $T_{\rm tr}$ as shown in inset. The interplay between the adiabaticity rate and finite coherence time leads to coherence maxima appearing for intermediate transition time, which for the chosen parameters is $T_{\rm tr} = 30$ ps. Hereafter the scaling factor of noise is $\beta = 0.05$, $\kappa = 0.1$ meV, and $\sigma = 3\gamma$.

In order to quantify the efficiency of the transition we calculate the coherence between the initially existing and the newly emerging interface states. As mentioned above, the interface state is mainly localised in 5 sites around the boundary between two phases. Accordingly, we introduce a vector describing this state

$$|\Psi_n(t)\rangle = \begin{pmatrix} \psi_{n,B} \\ \psi_{n,C} \\ \psi_{n,D} \\ \psi_{n+1,A} \\ \psi_{n+1,B} \end{pmatrix}. \tag{7}$$

Then the spatio-temporal first order correlation function between interface states can be defined as

$$g^{(1)}_{(n_b,\Delta n)}(\tau) = \frac{\langle \Psi^*_{n_b}(\tau_0)\Psi_{n_b+\Delta n}(\tau_0+\tau)\rangle_{\mathcal{N}}}{\sqrt{\langle|\Psi_{n_b}(\tau_0)|^2\rangle_{\mathcal{N}}\langle|\Psi_{n_b+\Delta n}(\tau_0+\tau)|^2\rangle_{\mathcal{N}}}}, \tag{8}$$

Optics EXPRESS

where $\Delta n = 0, 1, 2, \ldots$ corresponds to a shift of the interface state by respective number of unit cells, $\tau = t - \tau_0$ is the time interval. Here the average $\langle \ldots \rangle_{\mathcal{N}}$ is performed over a large number $\mathcal{N}$ of stochastic realizations. In all our simulations we use $\mathcal{N} = 1000$.

2.3. Results

Numerical simulations were performed for the model of an exciton-polariton lattice, where the tunnelling rate is chosen as $\kappa = 0.1$ meV. All the other quantities in the Hamiltonian are scaled relative to κ. Correspondingly, the temporal evolution is presented in ps. The parameter d in the definition of white noise corresponds to the diameter of the micropillar, and is chosen as $d = 3$ μm. The supporting on-site potential is $\sigma = 3\gamma$, and the scaling factor of noise amplitude is chosen as $\beta = 0.05$, corresponding to characteristic coherence time for polariton condensates [52]. The dependence of coherence degree on β is discussed in Appendix B.

In Fig. 2 we present the evolution of the first order correlation function of (8) during a shift of a interface state by one unit cell, for different switching rates. We start at $t = 0$ and perform the evolution for 500 ps with time independent Hamiltonian, during which we reach the nonequilibrium steady state. Note that from here onward, in all figures this part of the evolution is not shown. Then we gradually change the potentials in the boundary unit cells n_b and $n_b + 1$. The process is analogous to Landau-Zener transition [53,54]. One can expect that the lower is the transition speed, the higher will be the preserved degree of coherence due to a smaller perturbation of the steady state. This indeed is the case when increasing the switching time T_{tr} from 1 to 30 ps. However, due to non-Hermiticity of the Hamiltonian, the system is intrinsically of open-dissipative nature. This circumstance imposes a finite coherence time even in the steady state, stemming from the noise associated with input and output channels. In the context of exciton-polaritons these channels are represented by external incoherent pump and the finite lifetime of polaritons [29]. Correspondingly, the finite coherence time imposes the upper limit on

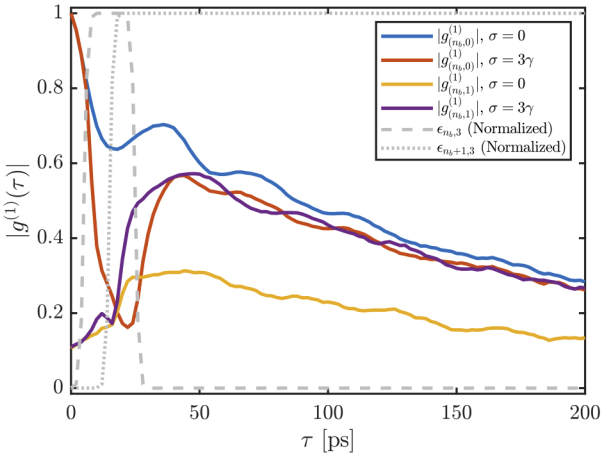

Fig. 3. The influence of supporting pump on coherence. The orange and purple curves show the evolution of correlation function in the absence and presence of supporting pump, respectively. The gray dashed and dotted lines correspond to temporal profiles of supporting pump and pump switching in the boundary unit cell. For comparison we show the evolution of local coherence in the scenario when no transition happens. The red curve corresponds to the presence of supporting pump, and the blue curve to its absence. The supporting pump in this case distorts the established steady state, and impose an additional noise. Hereafter $T_{\mathrm{tr}} = 30$ ps.

Optics EXPRESS

the transition period. Thus, the interplay of these two factors determines the timescale optimal for coherent transfer of the interface state to the next unit cell.

We further analyse the impact of the supporting on-site potential applied during the transfer protocol, defined by Eqs. (5) and (6). In Fig. 3 we present the temporal evolution of the coherence degree in the presence and absence of the potential. First of all we study coherence in the absence of switching, i.e. $g_{n_b,0}(\tau)$. Blue and red curves correspond here to $g_{n_b,0}(\tau)$ with and without applying supporting potential, respectively. We note that the additional noise stemming from the supporting potential largely reduces coherence. On the contrary, the coherence in the case of shift by one unit cell $[g_{n_b,1}(\tau)]$ is found to be very small in the absence of the supporting potential (see orange curve) whereas its presence allows to essentially preserve the coherence degree (purple line). It is remarkable that after the switching event, the degree and temporal evolution of the shifted interface state coherence (purple curve) is very close to that of coherence in the absence of switching (blue curve). This is another clear indication that the coherence is retained during the interface state transfer event.

In addition, we consider temporal dependence of the first order correlation function in the case of two consequent switching events, as shown in Fig. 4. The two switching events are separated by a large temporal window, during which the initial interface state becomes depleted, and the newly established interface state reaches to quasi steady state. Interestingly, the temporal

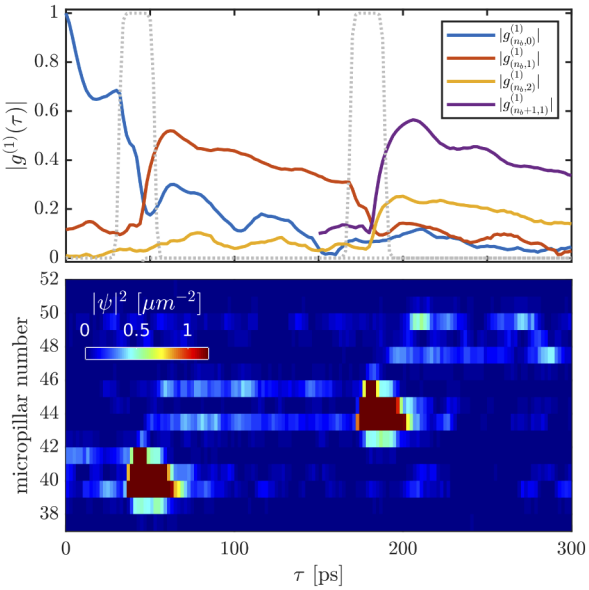

Fig. 4. The evolution of coherence (top panel) and population (bottom panel) during a two switch transfer. The two switching events are separated by a large temporal window (between 60 and 170 ps), which is necessary for the establishment of steady state after the first switch. The blue curve in top panel shows the temporal dependence of spatially local first order correlation function in the initial interface state. At the end of the saturation window it tends to zero, due to the complete depletion of population in the initial interface state (see the bottom panel). Some revival during the second switching event is an artifact of stochastic simulations. The red and purple curves correspond to the coherence between initial and intermediate (red), and intermediate and final interface states (purple). The very similar shape of these curves indicates that the two switching events are identical. The orange curve shows the correlation function between the initial and final interface states. The gray dotted lines correspond to temporal profiles of supporting pumps during the switching events.

Optics EXPRESS

profiles of the correlators $g_{n_b,1}$, $g_{n_b+1,1}$ [red and purple curves in Fig. 4(a)] are almost identical, indicating that the two switching events have same nature. Finally, after the second transition the correlator $g_{n_b,2}$ [orange curve in Fig. 4(a)] reaches the maximum value of 0.25. Evidently, this value shows that for the chosen parameters the multiple transitions will completely wash out the initial coherence.

In order to increase the conservation of coherence during the multiple transitions it is necessary the decrease the strength of the noise. However, in a realistic polariton model the latter has a limited range of allowed values. The dependence of coherence on scaling of the noise amplitude is discussed in Appendix B. A possible alternative could be the variation of the strength of supporting on-site potential. The dependence of coherence on the strength of supporting potential is shown in Fig. 5. The enhancement of supporting potential amplitude prevents the existing interface state from depletion, increasing thus the conservation of coherence. On the other hand, the stronger the pump, the more noise is introduced into the system, decreasing the coherence. The interplay of these factors determines the optimal rate of supporting potential $\sigma = 3\gamma$, which is used in majority of the calculations.

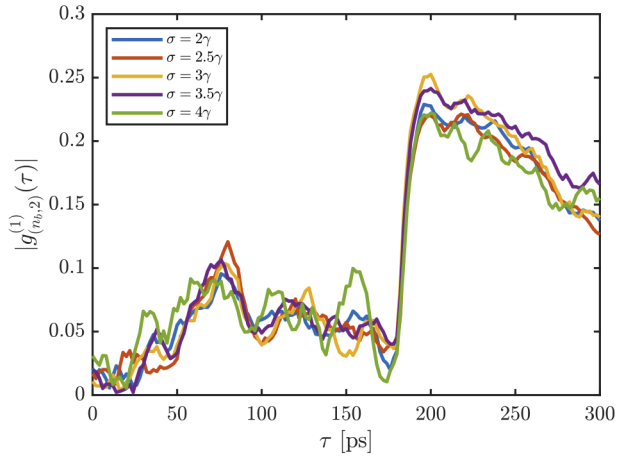

Fig. 5. Evolution of spatio-temporal correlation function during the shift of interface state by two cells for different values (in units of κ) of the amplitude of supporting on-site potential. The enhancement of supporting potential prevents the existing interface state from depletion. On the other hand, it is an additional source of noise. The interplay of these factors determines the optimal rate of supporting potential to be $\sigma = 3\gamma$.

3. Conclusion

In conclusion, we show the possibility of controllable coherent transport of topological interface states in a system of coupled Bose-Einstein condensates. We found that topologically protected interface state emerges solely due to spatial modulation of complex-valued on-site potential, while its temporal modulation causes the transfer of interface state. As a toy model we employ a system of interacting exciton-polariton condensates, where the on-site potential stems from the incoherent pump, and its spatial modulation provides the topological protection. We demonstrate that for the high purity systems with low noise amplitude a substantial coherence rate can be retained within a long-range transfer path, being an important prerequisite for practical applications.

Optics EXPRESS

Appendix A: polariton model

A possible system for the realization of the proposed phenomena is a one-dimensional (1D) lattice of coupled micropillars [9]. Each micropillar contains a quantum well and is assumed to host a tightly bound exciton-polariton mode. In the mean-field approximation the evolution of the system can be described by discrete mean-field Gross-Pitaevskii equations

$$\begin{aligned} i\hbar\dot{\psi}_{n,i} &= -\kappa \sum_{\langle nn\rangle} \psi_{n',i'} + \left[g_R n^R_{n,i} + i\frac{Rn^R_{n,i} - \gamma_c}{2} \right] \psi_{n,i}, \\ \dot{n}^R_{n,i} &= P_{n,i} - \left(\gamma_R + R|\psi_{n,i}|^2 \right) n^R_{n,i}, \end{aligned} \tag{9}$$

where $\psi_{n,i}(t)$ is the condensate amplitude in the n-th lattice cell, $n^R_{n,i}(t)$ is the density of exciton reservoir in the n,i-th site, $P_{n,i}$ is the external nonresonant pumping rate, γ_c and γ_R are the decay rates of the condensate and the reservoir, respectively, g_c and g_R are the corresponding interaction constants, and R is the rate of scattering from the reservoir to the condensate. We assume that the polariton interactions within the condensate are negligible in comparison with the reservoir-condensate interaction $g_R n^R_{n,i}$, which is a good approximation in most experiments where nonresonant pumping is used.

In the adiabatic approximation [55] we can write

$$n^R_{n,i} = \frac{P_{n,i}}{\gamma_R + R|\psi_{n,i}|^2} \approx \bar{n}^R_{n,i} - \frac{R}{\gamma_R}\bar{n}^R_{n,i}|\psi_{n,i}|^2 + O(|\psi_{n,i}|^4), \tag{10}$$

where $\bar{n}^R_{n,i} = P_{n,i}/\gamma_R$. The on-site potential in Eq. (2) stems from the linear terms in Eq. (9). In particular, we have

$$\left(g_{n,i} - \frac{\gamma}{\sin\theta} \right) e^{i\theta} = g_R \bar{n}^R_{n,i} + \frac{i}{2}\left(R\bar{n}^R_{n,i} - \gamma_c \right) = \left(\bar{n}^R_{n,i} - \frac{\gamma_c}{R} \right) \left(g_R + \frac{i}{2}R \right) + \frac{g_R\gamma_c}{R}. \tag{11}$$

The last term in the above expression is a constant real energy shift, which can be removed by introducing a rotating frame for condensate amplitudes, $\psi_{n,i} \to \psi_{n,i} e^{-i(g_R\gamma_c/R)t}$. Correspondingly, the term $\gamma\cot\theta$ is not present in Eq. (2) of the main text, as it only leads to irrelevant uniform energy shift. Thus, we introduce the following notations for linear and nonlinear terms

$$g_{n,i}e^{i\theta} - i\gamma \equiv \left(\bar{n}^R_{n,i} - \frac{\gamma_c}{R} \right) \left(g_R + \frac{i}{2}R \right), \tag{12}$$

and

$$\Gamma_{n,i} \equiv \frac{R}{\gamma_R}\bar{n}^R_{n,i}, \tag{13}$$

In the first of Eqs. (9) pumping of the condensate is represented by the term $Rn^R_{n,i}$, and losses by the decay rate γ_c. Considering quantum fluctuations only, the noise density is the sum of noise associated with these channels. Using Eq. (12), one has

$$R\bar{n}_{n,i} + \gamma_c = 2\left[\left(\bar{n}^R_{n,i} - \frac{\gamma_c}{R} \right) \frac{R}{2} + \gamma_c \right] = 2\left[g_n \sin\theta - \gamma + \gamma_c \right], \tag{14}$$

Thus, we obtain the density of quantum noise as

$$\langle \xi_{ni}(t)\xi^*_{n'i'}(t') \rangle = \delta_{nn'}\delta_{ii'}\delta_{tt'}\beta^2 2\left[g_n \sin\theta - \gamma + \gamma_c \right]/d. \tag{15}$$

Here d denotes the diameter of the micropillar, and β is dimensionless scaling parameter. The parameter β is introduced here because the above simple theoretical argument overestimates the

Optics EXPRESS

amplitude of quantum fluctuations. In our work, β is chosen to match the results of our simulations for the condensate coherence decay time with those reported in experimental investigations [52], i.e. the order of several hundreds of ps.

Finally, substituting the Eqs. (12), (13) into Eq. (9), and adding the noise term (15), we reach at the Eq. (2) of the main text.

Appendix B: scaling of the noise amplitude

Here we briefly discuss the dependence of first-order correlation function on the noise scaling factor β. For that, we study the temporal coherence of condensate in a single micropillar, defined as

$$g_0^{(1)}(\tau) = \frac{\langle \psi^*_{n,i}(\tau_0)\psi_{n,i}(\tau_0+\tau)\rangle_{\mathcal{N}}}{\sqrt{\langle |\psi_{n,i}(\tau_0)|^2\rangle_{\mathcal{N}}\langle |\psi_{n,i}(\tau_0+\tau)|^2\rangle_{\mathcal{N}}}}, \tag{16}$$

$\forall(n,i)$, and in the absence of hopping between the pillars, i.e. $\kappa = 0$. Figure 6 shows evolution of coherence for different values of β. As expected, the coherence decays exponentially, with the decay rate increasing together with noise amplitude.

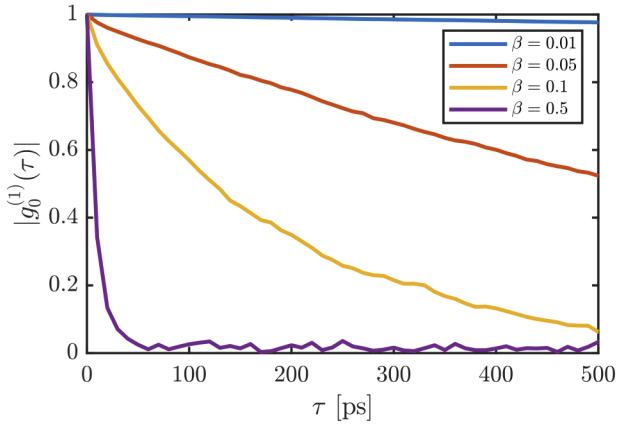

Fig. 6. The temporal evolution of condensate coherence in a single pillar defined by Eq. (16), for different scaling of the noise amplitude β.

Funding

Ministry of Education and Science of the Russian Federation (14.Y26.31.0015); Narodowe Centrum Nauki (2016/22/E/ST3/00045, 2017/25/Z/ST3/03032).

Acknowledgements

We acknowledge support from National Science Centre, Poland, grant No. 2016/22/E/ST3/00045 and grant No. 2017/25/Z/ST3/03032 under QuantERA program. VS acknowledges support from the mega-grant No. 14.Y26.31.0015 of the Ministry of Education and Science of the Russian Federation.

Disclosures

The authors declare no conflicts of interest.

Optics EXPRESS

References

1. M. Z. Hasan and C. L. Kane, "Colloquium: Topological insulators," Rev. Mod. Phys. **82**(4), 3045–3067 (2010).
2. C.-K. Chiu, J. C. Y. Teo, A. P. Schnyder, and S. Ryu, "Classification of topological quantum matter with symmetries," Rev. Mod. Phys. **88**(3), 035005 (2016).
3. Z. Gong, Y. Ashida, K. Kawabata, K. Takasan, S. Higashikawa, and M. Ueda, "Topological phases of non-hermitian systems," Phys. Rev. X **8**(3), 031079 (2018).
4. B. Bahari, A. Ndao, F. Vallini, A. El Amili, Y. Fainman, and B. Kanté, "Nonreciprocal lasing in topological cavities of arbitrary geometries," Science **358**(6363), 636–640 (2017).
5. M. A. Bandres, S. Wittek, G. Harari, M. Parto, J. Ren, M. Segev, D. N. Christodoulides, and M. Khajavikhan, "Topological insulator laser: Experiments," Science **359**(6381), eaar4005 (2018).
6. B. Midya, H. Zhao, and L. Feng, "Non-hermitian photonics promises exceptional topology of light," Nat. Commun. **9**(1), 2674 (2018).
7. K. Takata and M. Notomi, "Photonic topological insulating phase induced solely by gain and loss," Phys. Rev. Lett. **121**(21), 213902 (2018).
8. H. Zhao, X. Qiao, T. Wu, B. Midya, S. Longhi, and L. Feng, "Non-hermitian topological light steering," Science **365**(6458), 1163–1166 (2019).
9. P. Comaron, V. Shahnazaryan, W. Brzezicki, T. Hyart, and M. Matuszewski, "Non-hermitian topological end-mode lasing in polariton systems," Phys. Rev. Res. **2**(2), 022051 (2020).
10. D. Leykam, K. Y. Bliokh, C. Huang, Y. D. Chong, and F. Nori, "Edge modes, degeneracies, and topological numbers in non-hermitian systems," Phys. Rev. Lett. **118**(4), 040401 (2017).
11. S. Yao and Z. Wang, "Edge states and topological invariants of non-hermitian systems," Phys. Rev. Lett. **121**(8), 086803 (2018).
12. S. Yao, F. Song, and Z. Wang, "Non-hermitian chern bands," Phys. Rev. Lett. **121**(13), 136802 (2018).
13. F. K. Kunst, E. Edvardsson, J. C. Budich, and E. J. Bergholtz, "Biorthogonal bulk-boundary correspondence in non-hermitian systems," Phys. Rev. Lett. **121**(2), 026808 (2018).
14. H. Shen, B. Zhen, and L. Fu, "Topological band theory for non-hermitian hamiltonians," Phys. Rev. Lett. **120**(14), 146402 (2018).
15. V. M. Martinez Alvarez, J. E. Barrios Vargas, and L. E. F. Foa Torres, "Non-hermitian robust edge states in one dimension: Anomalous localization and eigenspace condensation at exceptional points," Phys. Rev. B **97**(12), 121401 (2018).
16. K. Yokomizo and S. Murakami, "Non-bloch band theory of non-hermitian systems," Phys. Rev. Lett. **123**(6), 066404 (2019).
17. K. Kawabata, S. Higashikawa, Z. Gong, Y. Ashida, and M. Ueda, "Topological unification of time-reversal and particle-hole symmetries in non-hermitian physics," Nat. Commun. **10**(1), 297 (2019).
18. M. Hafezi, E. A. Demler, M. D. Lukin, and J. M. Taylor, "Robust optical delay lines with topological protection," Nat. Phys. **7**(11), 907–912 (2011).
19. M. Hafezi, S. Mittal, J. Fan, A. Migdall, and J. Taylor, "Imaging topological edge states in silicon photonics," Nat. Photonics **7**(12), 1001–1005 (2013).
20. J. M. Zeuner, M. C. Rechtsman, Y. Plotnik, Y. Lumer, S. Nolte, M. S. Rudner, M. Segev, and A. Szameit, "Observation of a topological transition in the bulk of a non-hermitian system," Phys. Rev. Lett. **115**(4), 040402 (2015).
21. X. Zhan, L. Xiao, Z. Bian, K. Wang, X. Qiu, B. C. Sanders, W. Yi, and P. Xue, "Detecting topological invariants in nonunitary discrete-time quantum walks," Phys. Rev. Lett. **119**(13), 130501 (2017).
22. L. Xiao, X. Zhan, Z. Bian, K. Wang, X. Zhang, X. Wang, J. Li, K. Mochizuki, D. Kim, N. Kawakami, W. Yi, H. Obuse, B. C. Sanders, and P. Xue, "Observation of topological edge states in parity–time-symmetric quantum walks," Nat. Phys. **13**(11), 1117–1123 (2017).
23. S. Weimann, M. Kremer, Y. Plotnik, Y. Lumer, S. Nolte, K. G. Makris, M. Segev, M. C. Rechtsman, and A. Szameit, "Topologically protected bound states in photonic parity–time-symmetric crystals," Nat. Mater. **16**(4), 433–438 (2017).
24. M. Parto, S. Wittek, H. Hodaei, G. Harari, M. A. Bandres, J. Ren, M. C. Rechtsman, M. Segev, D. N. Christodoulides, and M. Khajavikhan, "Edge-mode lasing in 1d topological active arrays," Phys. Rev. Lett. **120**(11), 113901 (2018).
25. H. Zhao, P. Miao, M. H. Teimourpour, S. Malzard, R. El-Ganainy, H. Schomerus, and L. Feng, "Topological hybrid silicon microlasers," Nat. Commun. **9**(1), 981 (2018).
26. H. Zhou, C. Peng, Y. Yoon, C. W. Hsu, K. A. Nelson, L. Fu, J. D. Joannopoulos, M. Soljačić, and B. Zhen, "Observation of bulk fermi arc and polarization half charge from paired exceptional points," Science **359**(6379), 1009–1012 (2018).
27. N. A. Olekhno, E. I. Kretov, A. A. Stepanenko, P. A. Ivanova, V. V. Yaroshenko, E. M. Puhtina, D. S. Filonov, B. Cappello, L. Matekovits, and M. A. Gorlach, "Topological edge states of interacting photon pairs emulated in a topolectrical circuit," Nat. Commun. **11**(1), 1436 (2020).
28. S. D. Sarma, M. Freedman, and C. Nayak, "Majorana zero modes and topological quantum computation," npj Quantum Inf. **1**(1), 15001 (2015).
29. I. Carusotto and C. Ciuti, "Quantum fluids of light," Rev. Mod. Phys. **85**(1), 299–366 (2013).
30. C.-E. Bardyn, T. Karzig, G. Refael, and T. C. H. Liew, "Topological polaritons and excitons in garden-variety systems," Phys. Rev. B **91**(16), 161413 (2015).

Optics EXPRESS

31. O. Bleu, D. D. Solnyshkov, and G. Malpuech, "Interacting quantum fluid in a polariton chern insulator," Phys. Rev. B **93**(8), 085438 (2016).
32. R. Banerjee, T. C. H. Liew, and O. Kyriienko, "Realization of hofstadter's butterfly and a one-way edge mode in a polaritonic system," Phys. Rev. B **98**(7), 075412 (2018).
33. A. Janot, B. Rosenow, and G. Refael, "Topological polaritons in a quantum spin hall cavity," Phys. Rev. B **93**(16), 161111 (2016).
34. D. D. Solnyshkov, O. Bleu, B. Teklu, and G. Malpuech, "Chirality of topological gap solitons in bosonic dimer chains," Phys. Rev. Lett. **118**(2), 023901 (2017).
35. M. Sun, D. Ko, D. Leykam, V. M. Kovalev, and I. G. Savenko, "Exciton-polariton topological insulator with an array of magnetic dots," (2019).
36. A. V. Nalitov, D. D. Solnyshkov, and G. Malpuech, "Polariton $\mathbb{Z}$ topological insulator," Phys. Rev. Lett. **114**(11), 116401 (2015).
37. R. Ge, W. Broer, and T. C. H. Liew, "Floquet topological polaritons in semiconductor microcavities," Phys. Rev. B **97**(19), 195305 (2018).
38. V. K. Kozin, I. A. Shelykh, A. V. Nalitov, and I. V. Iorsh, "Topological metamaterials based on polariton rings," Phys. Rev. B **98**(12), 125115 (2018).
39. Y. V. Kartashov and D. V. Skryabin, "Two-dimensional topological polariton laser," Phys. Rev. Lett. **122**(8), 083902 (2019).
40. Y. V. Kartashov and D. V. Skryabin, "Bistable topological insulator with exciton-polaritons," Phys. Rev. Lett. **119**(25), 253904 (2017).
41. C. A. Downing, T. J. Sturges, G. Weick, M. Stobińska, and L. Martín-Moreno, "Topological phases of polaritons in a cavity waveguide," Phys. Rev. Lett. **123**(21), 217401 (2019).
42. C.-E. Bardyn, T. Karzig, G. Refael, and T. C. H. Liew, "Chiral bogoliubov excitations in nonlinear bosonic systems," Phys. Rev. B **93**(2), 020502 (2016).
43. H. Sigurdsson, G. Li, and T. C. H. Liew, "Spontaneous and superfluid chiral edge states in exciton-polariton condensates," Phys. Rev. B **96**(11), 115453 (2017).
44. H. Sigurdsson, Y. Krivosenko, I. Iorsh, I. Shelykh, and A. Nalitov, "Spontaneous topological transitions in a honeycomb lattice of exciton-polariton condensates due to spin bifurcations," Phys. Rev. B **100**(23), 235444 (2019).
45. P. St-Jean, V. Goblot, E. Galopin, A. Lemaître, T. Ozawa, L. Le Gratiet, I. Sagnes, J. Bloch, and A. Amo, "Lasing in topological edge states of a one-dimensional lattice," Nat. Photonics **11**(10), 651–656 (2017).
46. F. Baboux, E. Levy, A. Lemaître, C. Gómez, E. Galopin, L. Le Gratiet, I. Sagnes, A. Amo, J. Bloch, and E. Akkermans, "Measuring topological invariants from generalized edge states in polaritonic quasicrystals," Phys. Rev. B **95**(16), 161114 (2017).
47. M. Milićević, T. Ozawa, G. Montambaux, I. Carusotto, E. Galopin, A. Lemaître, L. Le Gratiet, I. Sagnes, J. Bloch, and A. Amo, "Orbital edge states in a photonic honeycomb lattice," Phys. Rev. Lett. **118**(10), 107403 (2017).
48. S. Klembt, T. Harder, O. Egorov, K. Winkler, R. Ge, M. Bandres, M. Emmerling, L. Worschech, T. Liew, M. Segev, C. Schneider, and S. Höfling, "Exciton-polariton topological insulator," Nature **562**(7728), 552–556 (2018).
49. C. E. Whittaker, E. Cancellieri, P. M. Walker, D. R. Gulevich, H. Schomerus, D. Vaitiekus, B. Royall, D. M. Whittaker, E. Clarke, I. V. Iorsh, I. A. Shelykh, M. S. Skolnick, and D. N. Krizhanovskii, "Exciton polaritons in a two-dimensional lieb lattice with spin-orbit coupling," Phys. Rev. Lett. **120**(9), 097401 (2018).
50. C. Gardiner, J. Anglin, and T. Fudge, "The stochastic gross-pitaevskii equation," J. Phys. B: At., Mol. Opt. Phys. **35**(6), 1555–1582 (2002).
51. S. Cockburn and N. Proukakis, "The stochastic gross-pitaevskii equation and some applications," Laser Phys. **19**(4), 558–570 (2009).
52. A. P. D. Love, D. N. Krizhanovskii, D. M. Whittaker, R. Bouchekioua, D. Sanvitto, S. A. Rizeiqi, R. Bradley, M. S. Skolnick, P. R. Eastham, R. André, and L. S. Dang, "Intrinsic decoherence mechanisms in the microcavity polariton condensate," Phys. Rev. Lett. **101**(6), 067404 (2008).
53. L. D. Landau, "Zur theorie der energieubertragung ii," Z. Sowjetunion **2**, 46–51 (1932).
54. C. Zener, "Non-adiabatic crossing of energy levels," Proc. R. Soc. Lond. A **137**(833), 696–702 (1932).
55. N. Bobrovska and M. Matuszewski, "Adiabatic approximation and fluctuations in exciton-polariton condensates," Phys. Rev. B **92**(3), 035311 (2015).